X-ray powder diffraction data for $ErH_{2-x}D_x$

Mark A. Rodriguez, Robert M. Ferrizz, and Clark S. Snow
Sandia National Laboratories, Albuquerque, New Mexico, 87185

James F. Browning
Oak Ridge National Laboratory, Oak Ridge, Tennessee, 37831

We report X-ray powder diffraction data for $ErH_{2-x}D_x$ formed by hydrogen (i.e. protium)-deuterium loading of Er metal. Lattice parameters for the varying hydrogen-deuterium compositions followed Vergard's law behavior. The cubic lattice parameter at room temperature for $ErH_{2-x}D_x$ obeys a linear relationship according to the formula **a** = 5.1287 $-1.1120 \cdot 10^{-4} \cdot x$; where **a** = the lattice parameter of the fluorite-type structure and x = the mole percent of deuterium. Microstrain measurements suggest a possible ordering of hydrogen and deuterium in the composition ErH_1D_1.

Keywords: Erbium hydride, ErD_2, ErH_2, X-ray diffraction (XRD), hydrogen, deuterium.

For submission to: Powder Diffraction

INTRODUCTION

Rare earth metal materials such as Er have long been of interest as a storage media of hydrogen (or protium) based on their ability to accommodate large concentrations of hydrogen within the metal lattice. Descriptions of the Er-H phase diagram have been outlined by Lundin (1968a, 1968b). His work discusses the stability of the fluorite-type structure of ErH_2 as well as its analog ErD_2. Erbium hydride compositions having the fluorite structure are often referred to as beta (β) phase compositions. In the erbium dihydride structure Er occupies the (0,0,0) corner site as well as the faces (½ ½ 0) of the face-centered cubic (FCC) lattice, while the hydrogen species occupy the tetrahedral sites at (¼ ¼ ¼). Multiplicity of these sites yields a total of 4 erbium atoms per cell along with 8 hydrogen atoms, for a chemical formula of ErH_2 where Z = 4 formula units per cell. There is a very minor difference in lattice parameter of the ErH_2 and ErD_2 structures due to isotopic effects. Deuterium is more massive than hydrogen and will therefore vibrate less, resulting in a smaller lattice parameter for the overall unit cell (Libowitz, 1965). This difference has been documented by Schleid & Meyer (1989) in which they synthesized ErH_2 and ErD_2 powders as precursor materials for the generation of $ErClH_x$ and $ErClD_{0.7}$ crystals. The minor difference in lattice parameter for ErD_2 and ErH_2 may prove important with respect to characterization of Erbium-based occluder materials. Hence, characterization of the variation of ErH_2 lattice parameter as a function of isotopic mixture of hydrogen vs. deuterium atoms would yield valuable benchmarks for determining H vs. D content. This evaluation is important because scattering from hydrogen isotopes via XRD is very weak and thereby structural occupancy determination

of hydrogen isotopes via XRD is rendered mute. However, by employing careful measurements of the lattice parameter, one can infer the ratio of hydrogen to deuterium within the host lattice via Vegard's law.

Table I documents the reported cell constants for entries in the Powder Diffraction File (PDF, 2007). From this table we notice that there is variation in the lattice parameter results for ErH_2. If one discounts the 5.09 Å value determined via electron diffraction (Oesterreicher, et al., 1978) the reported lattice parameter values for ErH_2 differ by no more than 0.6%. There is only one reported value for ErD_2 (Scheild & Meyer, 1989). This value is notably smaller than those for ErH_2 and Scheild & Meyer were successful in determining a difference between these two end member compositions for $ErH_{2-x}D_x$. However, only Oesterreicher, et al. (1978) reports tabular d/I data for ErH_2. All the other reported PDF entries are calculated based on the reported lattice parameter of the authors, which is inferred by the 999.9 value of the reported F_N figure-of-merit (Smith & Snyder, 1979) in Table I. While generating a calculated pattern for ErH_2 and ErD_2 is straight-forward for this FCC structure, it is difficult to judge which lattice parameter represents the most accurate value in the case of ErH_2. Because our research in this hydride system required very well determined values for the end member structures as well as predictive capabilities for mixed isotope compositions, we pursued the systematic study of $ErH_{2-x}D_x$ using careful synthesis and XRD analysis.

EXPERIMENTAL PROCEDURE

Bulk Erbium (99.99%) samples were hydrided using well-defined hydrogen/deuterium gas mixtures in a Sievert's-type apparatus (Ferrizz, et al., 2008). Samples were heated under vacuum to 500°C, "activated" for approximately 40 minutes, and then hydrided by exposure to the desired hydrogen/deuterium gas mixture. The H_2 and D_2 gas bottles used for the experiment were 99.99% grade purity. The reaction chamber was evacuated prior to sample cool down to room temperature. Analysis of system data during the loading process confirmed (via a mole balance calculation) the samples were loaded to the β phase dihdyride. This loading procedure was recently replicated via in-situ neutron diffraction (Rodriguez, et al., 2008), which confirmed full occupancy of the tetrahedral sites and absence of super-stoichiometric occupation of the octahedral (½ ½ ½) sites, thereby confirming the Er:H ratio of 1:2. As expected, the "bulk" erbium dihydride samples were easily ground into a powder after extraction from the loading apparatus.

A Siemens model D500 θ-2θ powder diffractometer (Bruker AXS, Inc. Madison, WI) was used for data collection with samples maintained at room temperature (25°C). Monochromatic Cu Kα (0.15406 nm) radiation was produced using a diffracted-beam curved graphite monochromator. Fixed slits were used, and the instrument power settings were 45 kV and 30 mA. Datascan V4.3 (Materials Data Inc.; Livermore, CA) software was used to operate the diffractometer.

Powder diffraction patterns were collected on a zero-background specimen holder according to the procedure outlined by Jenkins & Snyder, (1996a). The conditions for scans were as follows: 20-100° 2θ range, step-size of 0.04^o 2θ and a count-time of 2 sec. Initially, a LaB_6 (SRM 660) standard was run to confirm alignment of the instrument. In order to obtain the best possible peak positions, peaks were profile-fit using a Pearson VII peak-shape provided within the JADE software (version 8.0). These peak positions were employed to generate a theta calibration curve for subsequent analysis of $ErH_{2-x}D_x$ powders. To verify the proper function of the external calibration curve, the LaB_6 sample was run again. With the external theta calibration curve applied to the new pattern, the resulting refinement of the LaB_6 standard yielded a value of **a** = 4.1568(1) Å [F_{14} = 434.4 (Δ2θ = 0.0023^o, 14)] over the calibrated range of 25-100 ^{o}2θ, where F_{14} is the Smith and Snyder (1979) figure-of-merit (F_N). This measured value was within experimental error of the reported value for the LaB_6 powder (**a** = 4.15695(6) Å at 26°C (299 K).

Powder patterns for $ErH_{2-x}D_x$ powders were collected using the same zero-background holder as was used for the LaB_6 instrument calibration. As before with the LaB_6 analysis, profile-fitting employing the Pearson VII peak-shape was performed on $ErH_{2-x}D_x$ peaks. Each $ErH_{2-x}D_x$ peak was carefully fit using the same range of 2θ and identical starting parameter values [e.g., the (220) peak in each pattern was fit from 46.5 to 54.5 ^{o}2θ]. This systematic process was employed for all observed $ErH_{2-x}D_x$ powder patterns. Lattice parameter refinements and microstrain measurements for the $ErH_{2-x}D_x$ compounds were performed using JADE. Theta calibration of $ErH_{2-x}D_x$ powder patterns was performed using an external calibration function based on the LaB_6 standard; microstrain values

were derived from standard plots of B·Cos(θ) vs. Sin(θ) where B = the specimen broadening of the peak profile. The variation of peak broadening due to microstrain and crystallite size is easily derived from the equations documented by Jenkins and Snyder (1996b). These analyses employed the use of an instrument FWHM calibration also based on the LaB_6 standard.

RESULTS AND DISCUSION

The X-ray powder diffraction pattern for the ErH_1D_1 powder is shown in Figure 1 and is representative of all patterns obtained from the $ErH_{2-x}D_x$ series. This pattern is typical of fluorite-type structures, having the expected F*m-3m* symmetry. Lattice parameter refinements for the $ErH_{2-x}D_x$ compounds are shown in Table II. This table shows the lattice parameter contraction as deuterium content is increased into the fluorite structure. Figure 2 shows the linear relationship of lattice parameter contraction with mole % deuterium addition. The $ErH_{2-x}D_x$ series follows Vegard's law and can be described by the following formula:

(1) $$\mathbf{a} = 5.1287 - 1.1120 \cdot 10^{-4} \cdot x$$

where **a** is the lattice parameter and x is the mole percent deuterium.

Table II also shows some interesting variations for the microstrain measurements. To better illustrate the microstrain effects, Figure 3 plots the magnitude of microstrain as a function of $ErH_{2-x}D_x$ composition. Note that the compositions with uneven ratios of hydrogen and deuterium (i.e. $ErH_{1.5}D_{0.5}$ and $ErH_{0.5}D_{1.5}$) show significantly higher microstrain values as compared to the ErD_2 and ErH_1D_1 compositions (the ErH_2 composition will be discussed shortly). The implication from these data are that mixing

of the hydrogen and deuterium within the fluorite structure causes increased strain on the lattice due to the small difference in isotopic behavior. However, the dramatic drop in microstrain at ErH_1D_1 would imply that there is a mechanism for relief of the microstrain generated by equal mixing of the isotopes. We speculate that there is an ordering of the isotopes at the ErH_1D_1 composition which acts to reduce the strain in the lattice. However, due to the low scattering of the hydrogen and deuterium isotopes, superlattice peaks are not discernable in the XRD data. It is worth mentioning here that these measurements were done at room temperature. There is precedent for isotopic ordering within this system; however, it typically occurs at low temperature and in super-stoichiometric compositions (Vajda and Daou, 1994; Udovic, et al., 2000; Ratishvili and Vajda, 1996). It may be possible to confirm a structural ordering in ErH_1D_1 via neutron diffraction studies if the hydrogen scattering is not too problematic. This is an area of future research interest.

With regard to the ErH_2 composition, one may note that its microstrain value is nearly the same magnitude as that of the mixed $ErH_{0.5}D_{1.5}$ composition. There may be two trends occurring within these data. The first, as discussed above, is that uneven mixing of hydrogen/deuterium yields increased microstrain ($ErH_{1.5}D_{1.5}$ and $ErH_{0.5}D_{1.5}$ compositions). The second trend can be seen if we strictly consider ErH_2, ErH_1D_1 and ErD_2 compositions. In this case, the increased presence of hydrogen in the lattice tracks with increased microstrain, even when we do not consider mixing effects. Thus, it appears that the increased vibration of hydrogen as compared to deuterium results in more microstrain within the lattice and that microstrain may be further increased by the

presence of disorder of the isotopes within the structure due to uneven ratios of hydrogen/deuterium.

Results of lattice parameter refinement of the individual peaks in each powder pattern are shown for the various $ErH_{2-x}D_x$ compositions and are displayed in tabular format in Tables III-VII. Error for individual refined peak positions in terms of $\Delta 2\theta$ ($2\theta_{calc}$ - $2\theta_{obs}$) were generally very low, with most peaks displaying an error < 0.01^o 2θ and only one peak exceeding 0.02^o 2θ, the weak intensity (400) peak for $ErH_{1.5}D_{0.5}$ ($\Delta 2\theta = 0.023^o$ 2θ). The quality of the refinements is born out in the reported figure-of-merit values (see Table II) for the series. All samples refined to F_N values well above 100.

Tables III-VII also report relative intensity values observed for the sample series. These values are reported alongside calculated relative intensities generated using the program PowderCell (Ver. 2.4). Note all patterns share the same relative intensities for given hkl values because the hydrogen vs. deuterium content in the structure has negligible effect on relative intensities of the observed peaks. There are clear deviations observed for the measured intensities as compared to the expected values based on the powder pattern simulation. Note that the peaks beyond the (111) 100% peak are always underestimated when compared to the calculated values. The deviation in terms of percent underestimation tends to get worse with increased 2θ angle.

There are several possible effects that could generate loss of peak intensity and thereby inconsistent relative intensity values. These factors include preferred orientation effects,

detector dead-time problems, and lack of infinitely thick specimens. Due to the small quantity of material and the use of a scintillation detector, it is very unlikely that dead-time is a factor. With regard to a possible (111) preferred orientation, we did not observe the expected overestimation of the (222) peak in our diffraction data. Hence, the data are best explained as due to a lack of infinitely thick specimens in terms of penetration depth. Figure 4 illustrates this decay phenomenon. This graph plots the measured relative intensity as a ratio to the calculated relative intensity for a given hkl. For example, Table III shows that for the (220) hkl the observed I_{rel} = 27 % while the calculated I_{rel} = 35.6 %. The ratio 27/35.6 = 0.758. This number represents the underestimation of the (220) peak from its expected value for an infinitely thick specimen. One can calculate the decay for various thicknesses of the powder specimen (Cullity, 1978). The solid and dashed lines in Figure 4 illustrate the predicted drop-off (decay) of measured intensity for erbium dihydride as a function of 2θ for 5 μm and 3 μm thick powder specimens, respectively. The general trend of observed intensities is consistent with the modeled thicknesses of 3-5 μm thick specimens. Hence, we report the calculated relative intensities for the series as a better representation of I_{rel} values for this $ErH_{2-x}D_x$ series. All additional variation in the observed intensities from pattern to pattern can be considered statistical scatter typical of XRD measurements.

AKNOWLEDGMENT

Sandia is a multiprogram laboratory operated by Sandia Corporation, a Lockheed Martin Company, for the United States Department of Energy's National Nuclear Security Administration under contract DE-AC04-94AL85000.

REFERENCES

Bonnet, J. E. and Daou, J. N. (1977). "Rare-earth dihydride compounds: Lattice thermal expansion and investigation of the thermal dissociation," *J. Appl. Phys*., **48**, pp. 964-968.

Cullity B. D. (1978). Elements of X-Ray Diffraction, 2nd ed., Addison Westley, Reading, Massachusetts, pp.292.

Ferrizz, R. M.; Louck, T. J. and King, S. H. (2008). "PCT Apparatus: Overview," internal report number SAND2007-8105, Sandia National Laboratories, Albuquerque, NM, 87185 and Livermore, CA, 94550.

Jenkins, R. and Snyder, R. L. (1996a). Introduction to X-ray Powder Diffractometry, John Wiley & Sons, New York, pp. 249.

Jenkins, R. and Snyder, R. L. (1996b). Introduction to X-ray Powder Diffractometry, John Wiley & Sons, New York, pp. 89-94.

Libowitz, G. (1965). The solid-state chemistry of binary metal hydrides, W. A. Benjarmin Inc., New York, pp. 27.

Lundin, C. E. (1968a). "The erbium-hydrogen system," *Transactions of the Metallurgical Society of AIME*, **242**, pp. 903-907.

Lundin, C. E. (1968b). "Thermodynamics of the erbium deuterium system." *Transactions of the Metallurgical Society of AIME*, **242**, pp. 1161-1165.

Oesterreicher, H.; Bittner, H. and Kothari, B. (1978). "Laser evaporation and condensation of Er in hydrogen and inert atmosphere," *J. Solid State Chem*., **26**, pp. 97-99.

PDF (2007). PDF-4+ 2007 RDB 4.0707; International Centre for Diffraction data, Newtown Square, PA.

Pebler, A. and Wallace, W. E. (1962). "Crystal structure of some lanthanide hydrides," *J. Phys. Chem*., 66, pp. 148-151.

Ratishvili, I. G. and Vajda, P. (1996). "Hydrogen ordering in superstoichiometric rare-earth hydrides for a system with an energy-constants ratio $p=V_2/V_1 < 1$: LaH_{2+x}," *Phys. Rev. B*, **53**, pp. 581-587.

Rodriguez, M. A.; Snow, C.; Wixom, R., Llobet, A., and Browning, J. F. (2008). Manuscript in preparation.

Schleid, T. and Meyer, G. (1989). "Hydrogen(Deuterium)-Stabilized and Lithium-Intercalated Erbium Monochloride: An X-Ray Single-Crystal and Neutron Diffraction Study", *J. Less-Common Met*., **156**, pp. 161-171.

Smith, G. S. and Snyder, R. L. (**1979**). "F_N : Criteron for rating powder diffraction patterns and evaluating the reliability of powder-pattern indexing," J. Appl. Crystallogr. **12**, 60-65.

Udovic, T. J.; Huang, Q. and Rush, J. J. (2000). "Hydrogen and deuterium site separation in fcc-based mixed-isotope rare-earth hydrides," *Phys. Rev. B*, **61**, pp. 6611-6616.

Vajda, P. and Daou, J. N. (1994). "Magnetic and metal-semiconductor transitions in ordered and disordered $ErH(D)_{2+x}$," *Phys. Rev. B*, **49**, pp. 3275-3282.

Table I. PDF database information regarding ErH_2 and ErD_2 compounds

Reference	PDF entry	Compound	Lattice parameter (A)	F_N: Figure of Merit†
Pebler & Wallace (1962)	04-003-4752	ErH_2	5.123	F_{14} = 999.9
Bonnet & Daou (1977)	04-004-5083*	ErH_2	5.1279	F_{14} = 999.9
Oesterreicher, et. al. (1978)	00-047-0978	ErH_2	5.09	F_7 = 42.9
Schleid & Meyer (1989)	04-007-3134	ErH_2	5.1253	F_{14} = 999.9
Schleid & Meyer (1989)	04-007-3135	ErD_2	5.1137	F_{14} = 999.9

*same as entry 01-073-8648
†Smith and Snyder (1979)

Table II. Lattice parameter refinement data for $ErH_{2-x}D_x$ compounds

Formula	Mole % deuterium (error±2%)	Lattice Parameter (Å)	Cell Volume ($Å^3$)	X-ray Density (g/cm^3)	F_N Figure-of-Merit† F(9)	Average $\Delta 2\theta$ (^{o})	Microstrain (%)
ErH_2	0	5.1288(4)	134.91	8.336	209.7	0.0048	0.159(6)
$ErH_{1.5}D_{0.5}$	25	5.1256(4)	134.66	8.376	146.6	0.0068	0.183(6)
ErH_1D_1	50	5.1232(2)	134.47	8.413	430.8	0.0023	0.131(5)
$ErH_{0.5}D_{1.5}$	75	5.1204(3)	134.25	8.452	204.1	0.0049	0.171(6)
ErD_2	100	5.1175(5)	134.02	8.491	306.6	0.0033	0.124(5)

All refined parameter errors are 3σ of the reported values of refinement outputs
†Smith and Snyder (1979)

Table III. X-ray powder diffraction data for ErH_2.
Radiation: Cu $K\alpha_1$ (0.15406 nm)

hkl	2θ calc (°)	2θ obs (°)	Δ2θ (°)	d calc (Å)	d obs (Å)	I calc (%)	I obs (%)
111	30.156	30.155	0.001	2.9611	2.9612	100	100
200	34.961	34.959	0.002	2.5644	2.5646	48.8	42
220	50.276	50.281	-0.006	1.8133	1.8131	35.6	27
311	59.752	59.754	-0.003	1.5464	1.5463	39.7	27
222	62.701	62.703	-0.002	1.4806	1.4805	11.0	8
400	73.848	73.858	-0.010	1.2822	1.2821	5.0	3
331	81.788	81.786	0.002	1.1766	1.1767	14.6	10
420	84.392	84.376	0.016	1.1468	1.1470	13.3	9
422	94.745	94.747	-0.002	1.0469	1.0469	10.3	6

Table IV. X-ray powder diffraction data for $ErH_{1.5}D_{0.5}$.
Radiation: Cu $K\alpha_1$ (0.15406 nm)

hkl	2θ calc (°)	2θ obs (°)	Δ2θ (°)	d calc (Å)	d obs (Å)	I calc (%)	I obs (%)
111	30.176	30.176	-0.001	2.9593	2.9592	100	100
200	34.984	34.982	0.002	2.5628	2.5629	48.8	44
220	50.310	50.313	-0.003	1.8122	1.8121	35.6	32
311	59.793	59.799	-0.005	1.5454	1.5453	39.7	33
222	62.745	62.745	0.000	1.4796	1.4796	11.0	10
400	73.903	73.880	0.023	1.2814	1.2817	5.0	4
331	81.851	81.833	0.017	1.1759	1.1761	14.6	11
420	84.458	84.453	0.005	1.1461	1.1462	13.3	10
422	94.824	94.818	0.006	1.0463	1.0463	10.3	8

Table V. X-ray powder diffraction data for ErH_1D_1.
Radiation: Cu $K\alpha_1$ (0.15406 nm)

hkl	2θ calc (°)	2θ obs (°)	Δ2θ (°)	d calc (Å)	d obs (Å)	I calc (%)	I obs (%)
111	30.190	30.189	0.001	2.9579	2.9580	100	100
200	35.000	35.002	-0.002	2.5616	2.5615	48.8	44
220	50.335	50.337	-0.002	1.8113	1.8113	35.6	33
311	59.824	59.824	0.000	1.5447	1.5447	39.7	34
222	62.778	62.779	-0.002	1.4789	1.4789	11.0	10
400	73.943	73.947	-0.004	1.2808	1.2807	5.0	4
331	81.897	81.896	0.001	1.1753	1.1754	14.6	13
420	84.506	84.505	0.001	1.1456	1.1456	13.3	10
422	94.882	94.875	0.008	1.0458	1.0458	10.3	8

TABLE VI. X-ray powder diffraction data for $ErH_{0.5}D_{1.5}$.
Radiation: Cu $K\alpha_1$ (0.15406 nm)

hkl	2θ calc (°)	2θ obs (°)	Δ2θ (°)	d calc (Å)	d obs (Å)	I calc (%)	I obs (%)
111	30.207	30.208	-0.002	2.9563	2.9561	100	100
200	35.020	35.020	0.000	2.5602	2.5602	48.8	46
220	50.364	50.364	0.000	1.8103	1.8103	35.6	35
311	59.859	59.861	-0.002	1.5439	1.5438	39.7	37
222	62.815	62.819	-0.004	1.4781	1.4781	11.0	11
400	73.989	73.984	0.005	1.2801	1.2802	5.0	5
331	81.950	81.947	0.003	1.1747	1.1747	14.6	13
420	84.562	84.552	0.010	1.1450	1.1451	13.3	12
422	94.950	94.931	0.019	1.0452	1.0454	10.3	10

TABLE VII. X-ray powder diffraction data for ErD_2.
Radiation: Cu $K\alpha_1$ (0.15406 nm)

hkl	2θ calc (°)	2θ obs (°)	Δ2θ (°)	d calc (Å)	d obs (Å)	I calc (%)	I obs (%)
111	30.224	30.225	0.000	2.9546	2.9546	100	100
200	35.041	35.037	0.003	2.5588	2.5590	48.8	41
220	50.395	50.396	-0.001	1.8093	1.8093	35.6	31
311	59.897	59.901	-0.004	1.5430	1.5429	39.7	31
222	62.855	62.858	-0.012	1.4773	1.4773	11.0	9
400	74.039	74.036	0.003	1.2794	1.2794	5.0	4
331	82.007	82.001	0.006	1.1740	1.1741	14.6	12
420	84.622	84.621	0.000	1.1443	1.1443	13.3	10
422	95.021	95.012	0.009	1.0446	1.0447	10.3	8

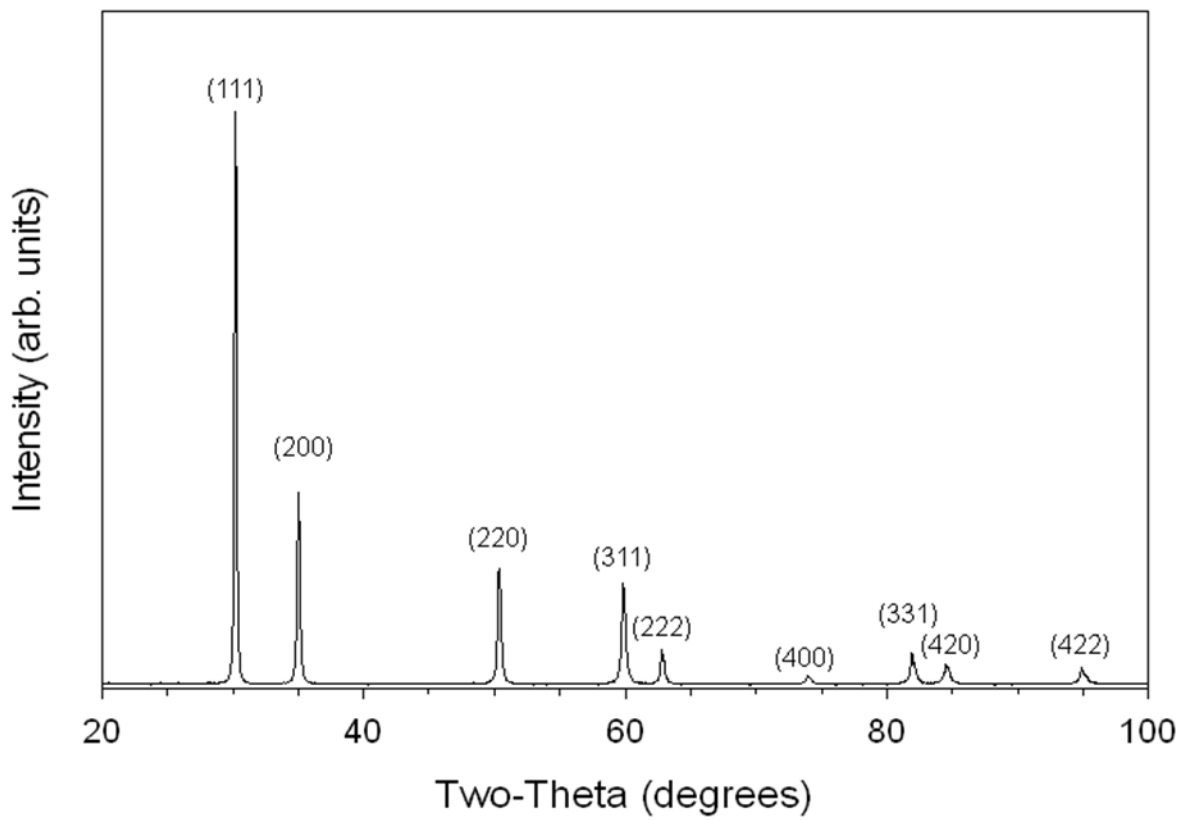

Figure 1. Observed powder X-ray diffraction pattern for the ErH_1D_1 compound in the series $ErH_{2-x}D_x$.

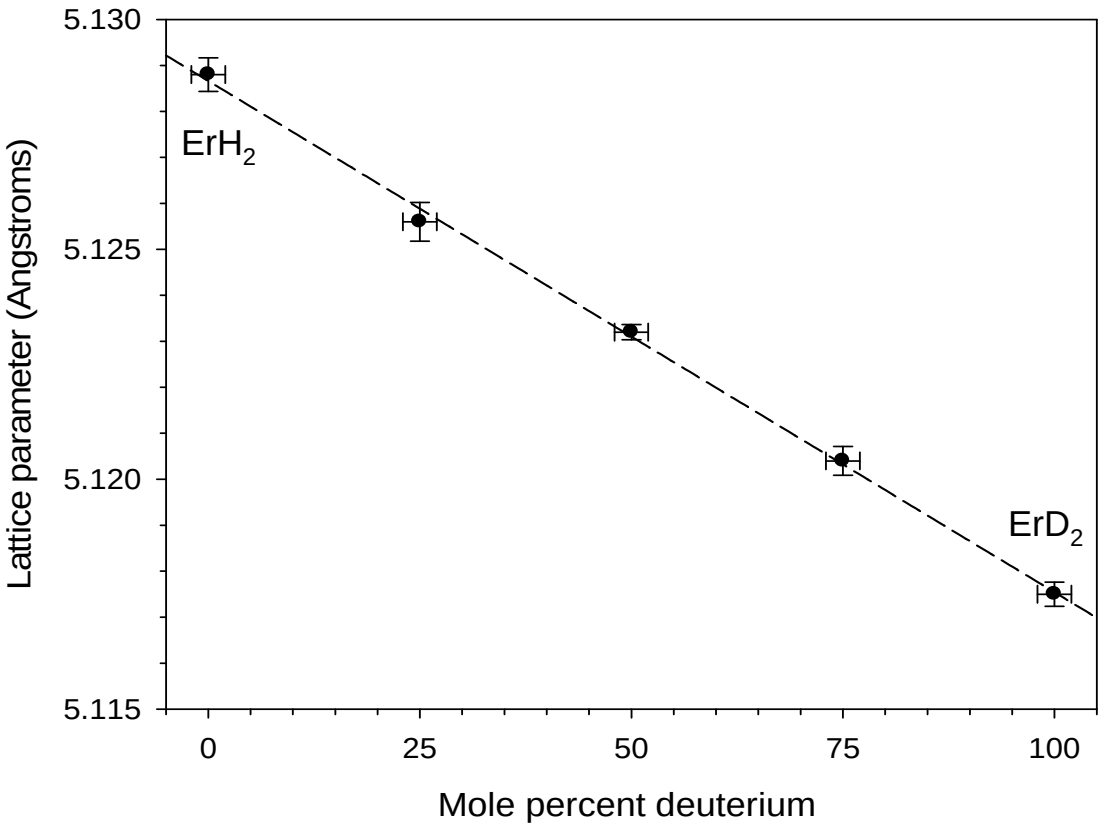

Figure 2. Lattice parameters for the series $ErH_{2-x}D_x$ as a function of mole percent deuterium.

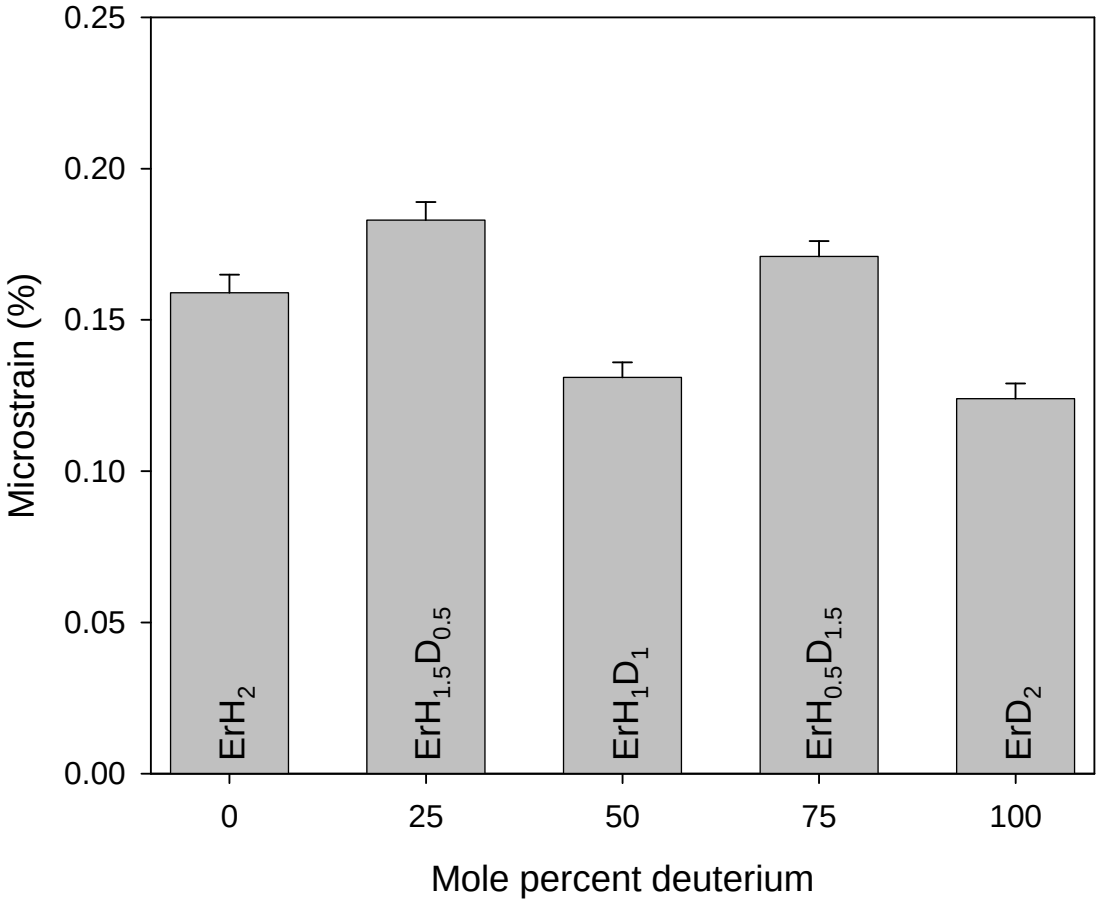

Figure 3. Microstrain as a function of composition. See text for details.

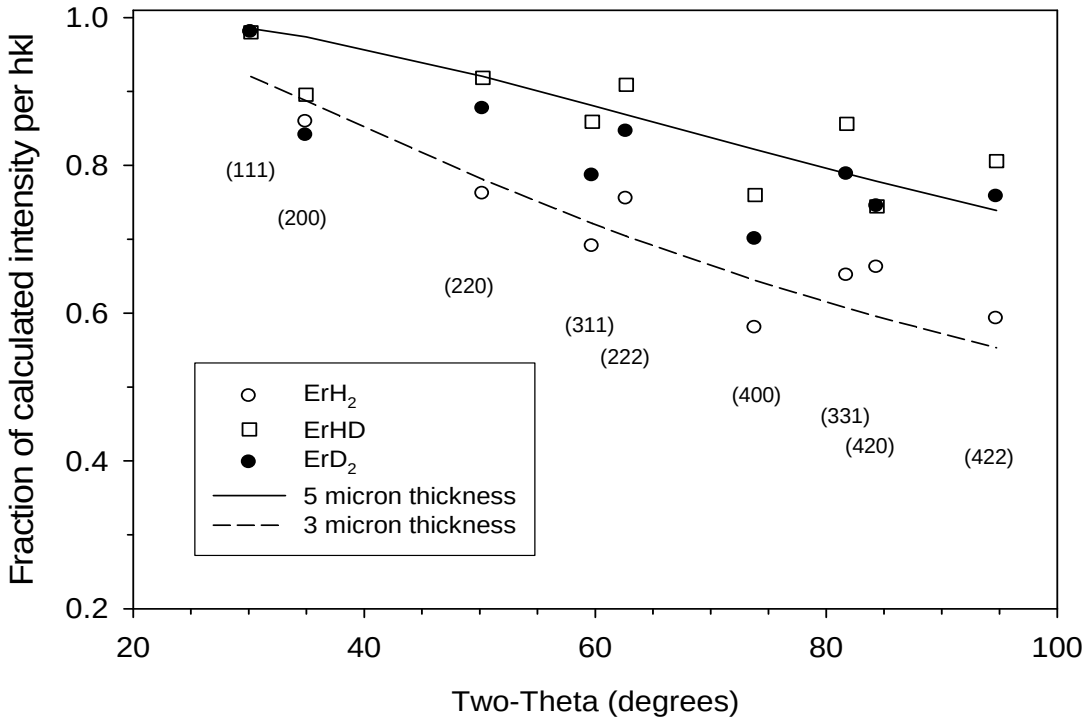

Figure 4. Decay of peak intensity as compared to calculated intensity for various powders. Lines represent expected decay curves due to lack of infinitely thick specimen. See text for details.